



ELSEVIER

Available online at [www.sciencedirect.com](http://www.sciencedirect.com)

SCIENCE @ DIRECT®

Applied Surface Science 207 (2003) 246–254

applied  
surface science

[www.elsevier.com/locate/apsusc](http://www.elsevier.com/locate/apsusc)

# Oxidation behaviour of Kanthal A1 and Kanthal AF at 1173 K: effect of yttrium alloying addition

R. Cueff<sup>\*</sup>, H. Buscail, E. Caudron, C. Issartel, F. Riffard

*Laboratoire Vellave sur l'Elaboration et l'Etude des Matériaux, Equipe locale Université Blaise Pascal Clermont-Ferrand II, BP 219, 43006 Le Puy-en-Velay Cedex, France*

Received 11 November 2002; received in revised form 2 December 2002; accepted 2 December 2002

## Abstract

The oxidation behaviour of two commercial FeCrAl alloys, Kanthal A1 and Kanthal AF (containing alloying additions of yttrium), has been investigated during isothermal exposures in air at 1173 K. Mass gains were measured by thermogravimetry and identification of the oxidation products determined by in situ high temperature X-ray diffraction. The morphology of the oxide layer surfaces was studied by SEM, the elemental distribution inside the scales being carried out by EDXS analysis. The study revealed that yttrium markedly influences the composition and growth rate of the oxide scale during the steady-state stage of oxidation. The lower oxidation rate resulting from the presence of the reactive element reflects the influence of yttrium in suppressing the formation of transition alumina and promoting the earlier formation of a protective  $\alpha$ -Al<sub>2</sub>O<sub>3</sub> scale.

© 2003 Elsevier Science B.V. All rights reserved.

**Keywords:** FeCrAl alloys; Yttrium; Reactive element effect; High temperature oxidation; X-ray diffraction

## 1. Introduction

Alumina forming alloys present interesting anticorrosion properties under high temperature oxidizing environments. Their high aluminium content allows the formation of a protective  $\alpha$ -alumina scale. However, this oxide scale can be susceptible to spallation under thermal cycling. Many investigations have shown that the addition of reactive element (such as yttrium or cerium) to FeCrAl alloys improves their corrosion resistance at high temperature. Though the influence of yttrium on the oxidation of FeCrAl has been studied extensively [1–8], the mechanisms of this

reactive element effect are still a matter of discussion. The growth and development of protective Al<sub>2</sub>O<sub>3</sub> scales during oxidation at temperatures from 1073 to 1273 K is complicated by the presence of transition aluminas ( $\gamma$ -Al<sub>2</sub>O<sub>3</sub>,  $\delta$ -Al<sub>2</sub>O<sub>3</sub>,  $\theta$ -Al<sub>2</sub>O<sub>3</sub>) which transform into the stable  $\alpha$ -alumina. Many studies have reported that the influence of yttrium on the oxidation behaviour of an alumina forming alloy is related to its effect on the alumina phase transformation [9–13]. The modes of introduction of the reactive element include alloying additions of the reactive element or its oxide, ion implantation of the element and superficial application of the reactive element oxide as a thin coating (sol–gel, electrophoresis, MOCVD methods). The present work deals with the influence of yttrium alloying additions on the oxidation of alumina

<sup>\*</sup> Corresponding author. Fax: +33-04-71-09-90-49.  
E-mail address: [cueff@iut.u-clermont1.fr](mailto:cueff@iut.u-clermont1.fr) (R. Cueff).

forming alloys at 1173 K. Thus, the oxidation behaviour of two commercial FeCrAl alloys, Kanthal A1 and Kanthal AF (containing alloying additions of yttrium), is investigated, with emphasis placed on kinetics related to the scale structure evolution at high temperature.

## 2. Experimental methods

The chemical compositions (obtained by glow discharge optical spectroscopy) of the two FeCrAl alloys (produced by melting) are reported in Table 1. One millimeter thick specimens of rectangular shape with a total area of about 4 cm<sup>2</sup> were abraded with SiC paper up to 800 grade and ultrasonically cleaned in ethanol prior to oxidation. Oxidation kinetics were followed at 1173 K, in laboratory air, during 120 h, using a Setaram TGDTA 92-1600 thermobalance. In situ scale structure evolution was analysed in a high temperature Anton PAAR HTK 1200 chamber with an integrated sample spinner in a Philips X'pert MPD diffractometer. The X-ray diffraction (XRD) goniometer is equipped with a curved Cu monochromator to isolate the diffracted Cu K $\alpha$  wavelength from all other wavelengths such as iron fluorescence radiation. In situ XRD analyses were performed using Cu K $\alpha_1$  (0.15406 nm) radiation. Series of X-ray diffractograms were recorded every hour during the 30 h oxidation test. The most representative in situ XRD

spectra will only be presented in our study. Diffraction peaks will be considered as significant if their relative intensity is greater than 10% of the intensity reported on their corresponding Joint Committee on Powder Diffraction Standards (JCPDS) file. The oxide scale surface and cross-section morphologies were observed by scanning electron microscopy (SEM) coupled with energy dispersive X-ray spectrometry (EDXS). The EDXS point analyses were performed with an electron probe focused to a 1  $\mu$ m spot. For cross-section analyses, the specimens were mounted in resin before polishing (with 1  $\mu$ m diamond suspension) in order to preserve the integrity of the brittle oxide scales on the FeCrAl substrates. An evaporated carbon coating of about 10 nm thickness was also deposited on these samples to improve conducting properties.

## 3. Results

### 3.1. Oxidation kinetics

Fig. 1 presents the oxidation curves  $\Delta m/S = f(t^{1/2})$  of Kanthal A1 and Kanthal AF. It can be observed that the mass gain after 120 h oxidation is clearly higher for the yttrium-free specimen than for the yttrium-containing one. These mass gains are, respectively, 0.26 and 0.12 mg cm<sup>-2</sup>, for the Kanthal A1 and Kanthal AF specimens. In both cases, the kinetic curves exhibit an initial transient stage during the first hours, followed by a parabolic rate law. The two alloys show similar mass gains up to 6 h oxidation. On the contrary, after longer oxidation times, the oxidation rate of Kanthal A1 was significantly higher than that exhibited by Kanthal AF. The parabolic rate constants,  $k_p$ , are, respectively,  $1.3 \times 10^{-7}$  mg<sup>2</sup> cm<sup>-4</sup> s<sup>-1</sup> for Kanthal A1 and  $1.4 \times 10^{-8}$  mg<sup>2</sup> cm<sup>-4</sup> s<sup>-1</sup> for Kanthal AF. The kinetic results indicate that the yttrium-free and the yttrium-containing specimens are predominantly controlled by a diffusional process, though an interfacial process occurs during the first hours of the experiment. They also reveal that yttrium addition as alloying element in Kanthal AF does not have significant influence on the growth rate of the oxide scale during the early transient stage, whereas it shows a beneficial effect when the parabolic regime is established.

Table 1  
Composition of Kanthal A1 and Kanthal AF (wt.%)

Elements	Alloys	
	Kanthal A1	Kanthal AF
Fe	71.3	71.4
Cr	22.2	22.8
Al	5.66	5.23
Si	0.26	0.21
Mn	0.13	0.17
Zr	0.083	0.054
C	0.022	0.036
Ti	0.016	0.071
Y	<0.005	0.028
Ce	<0.005	<0.010
Mg	<0.005	<0.005
S	<0.005	<0.005
Hf	<0.005	<0.001

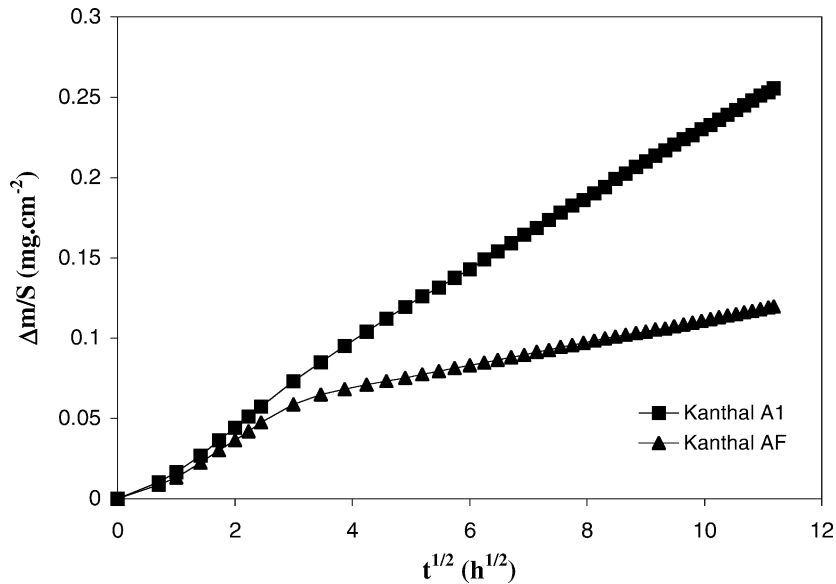


Fig. 1. Mass-gain versus square root of time for Kanthal A1 and Kanthal AF at 1173 K in air.

### 3.2. In situ high temperature XRD

#### 3.2.1. Oxidation of Kanthal A1

In situ high temperature XRD patterns obtained on Kanthal A1 specimen are given in Fig. 2. The relatively high intensity of the characteristic diffraction peaks of the FeCrAl alloy during the whole experiment suggests that the sample is slowly oxidized. The diffractograms clearly show that  $\alpha$ -Al<sub>2</sub>O<sub>3</sub> (JCPDS 46-1212) is formed during the first hours. The typical diffraction peaks of  $\alpha$ -Al<sub>2</sub>O<sub>3</sub> are detected after 2 h and their intensity increases continuously up to 30 h. The presence of transition aluminas,  $\delta$ -Al<sub>2</sub>O<sub>3</sub> (JCPDS 46-1131) and  $\theta$ -Al<sub>2</sub>O<sub>3</sub> (JCPDS 35-0121), is also detected after 7 h oxidation. The high intensity of the peak near  $2\theta = 37.7^\circ$  leads to the assumption that this peak does not contain only the  $\alpha$ -Al<sub>2</sub>O<sub>3</sub> (1 1 0) peak. It probably corresponds to the overlapping of the  $\delta$ -Al<sub>2</sub>O<sub>3</sub> (0 2 5) (JCPDS file relative intensity: 43%),  $\delta$ -Al<sub>2</sub>O<sub>3</sub> (1 2 3) (JCPDS file relative intensity: 38%),  $\delta$ -Al<sub>2</sub>O<sub>3</sub> (1 0 9) (JCPDS file relative intensity: 34%) and the  $\alpha$ -Al<sub>2</sub>O<sub>3</sub> (1 1 0) (JCPDS file relative intensity: 21%) diffraction peaks. All the experimental peaks which allow identification of  $\theta$ -Al<sub>2</sub>O<sub>3</sub> correspond to the overlapping of  $\theta$ -Al<sub>2</sub>O<sub>3</sub> and  $\delta$ -Al<sub>2</sub>O<sub>3</sub> diffraction peaks. Among them, the peak located near  $2\theta = 32.8^\circ$  exhibits the greatest intensity. It can be attributed to the overlapping of the

$\theta$ -Al<sub>2</sub>O<sub>3</sub> (2 0  $\bar{2}$ ) (JCPDS file relative intensity: 100%),  $\theta$ -Al<sub>2</sub>O<sub>3</sub> (2 0 0) (JCPDS file relative intensity: 100%),  $\delta$ -Al<sub>2</sub>O<sub>3</sub> (0 2 2) (JCPDS file relative intensity: 71%) diffraction peaks. This peak intensity increases significantly from 18 to 30 h oxidation, whereas the intensity of the  $\delta$ -Al<sub>2</sub>O<sub>3</sub> (2 2 0) peak located at  $2\theta = 45.6^\circ$  remains roughly constant during the same period. This relative evolution of the transition alumina characteristic diffraction peaks underlines the more pronounced evidence of the  $\theta$ -Al<sub>2</sub>O<sub>3</sub> presence during the last 10 h oxidation.

#### 3.2.2. Oxidation of Kanthal AF

As observed in the case of Kanthal A1, the diffractograms in Fig. 3 show that the yttrium-containing sample is slowly oxidized. This figure clearly indicates that the growth of  $\alpha$ -alumina starts from the beginning of the test, at least after the first diffractogram at 1 h exposure. The diffraction peaks of  $\alpha$ -Al<sub>2</sub>O<sub>3</sub> are clearly detected all along the 30 h oxidation test. It is interesting to note the absence of transition aluminas, which were coexisting with  $\alpha$ -Al<sub>2</sub>O<sub>3</sub> in the oxide scale formed on Kanthal A1. Yttrium seems to suppress the formation of transition alumina and favours early  $\alpha$ -Al<sub>2</sub>O<sub>3</sub> formation and growth. However, the in situ XRD analysis has not allowed the identification of any yttrium or yttrium–aluminium oxides.

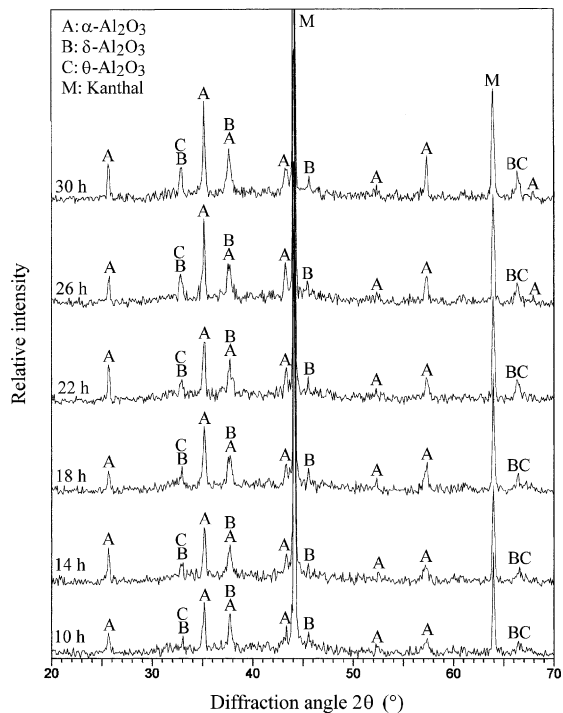
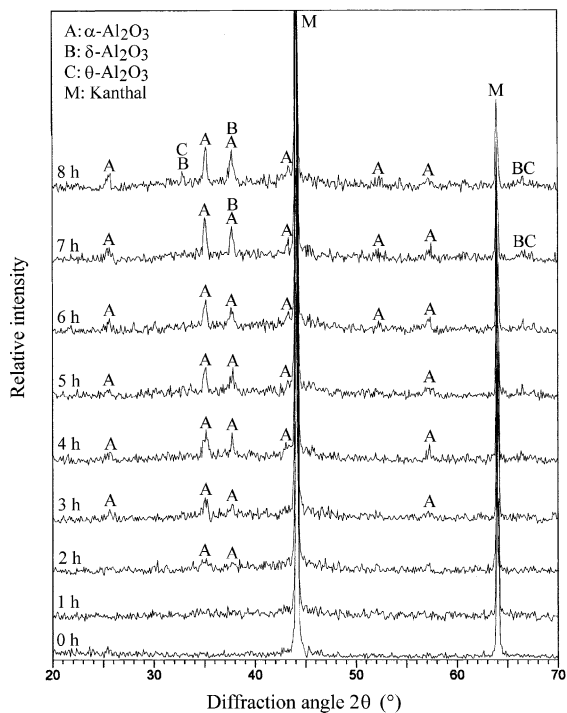


Fig. 2. Selected in situ XRD patterns performed on Kanthal A1 at 1173 K in air (0–30 h).

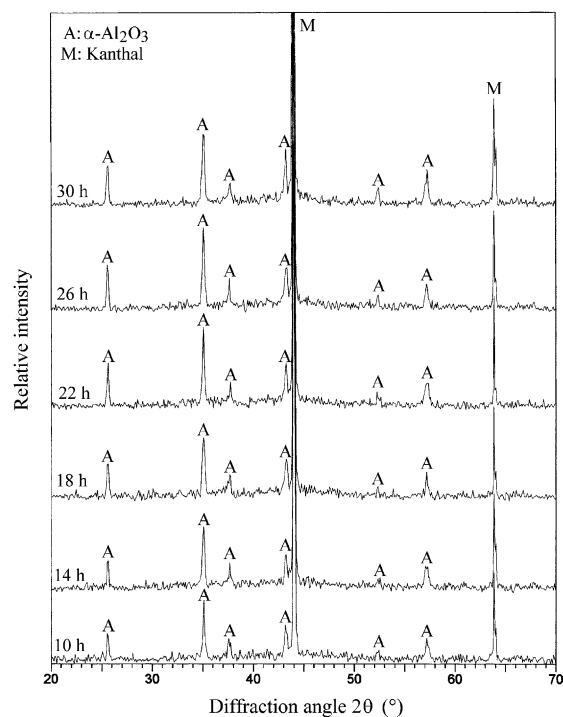
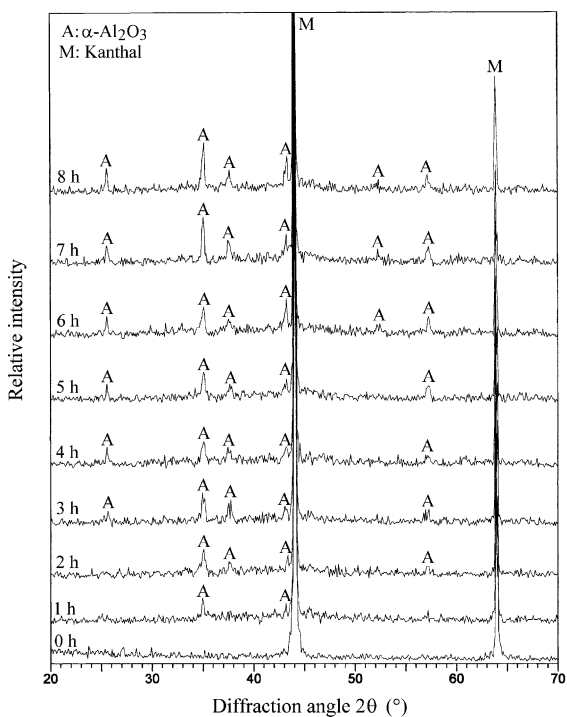


Fig. 3. Selected in situ XRD patterns performed on Kanthal AF at 1173 K in air (0–30 h).

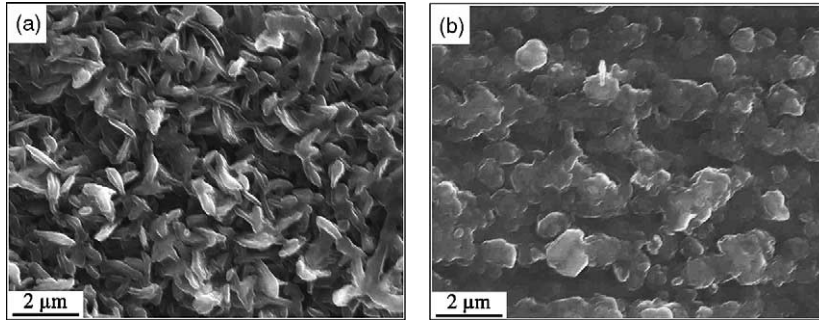


Fig. 4. Surface scale morphology (SEM secondary electron images) of Kanthal A1 (a), Kanthal AF (b), and oxidized in air at 1173 K.

Nevertheless, we cannot reliably conclude the absence of the reactive element in the oxide scale since its concentration can be below the detection limit of XRD. Other authors also reported that X-ray diffractograms of Kanthal AF oxidized at high temperature only revealed alumina and the metal substrate [14], whereas other studies noted for a similar FeCrAl alloy, the presence of sparse precipitates containing small amounts of zirconium, titanium and yttrium in an  $\alpha$ - $\text{Al}_2\text{O}_3$  layer [15].

### 3.3. Oxide scale morphology

The scale surface morphology is strongly affected by the scale composition. On the one hand, Fig. 4a shows the blade-like whiskers morphology of the outer surface of the oxide scale developed on the yttrium-free alloy. This typical morphology appears to be

indicative of  $\theta$ - $\text{Al}_2\text{O}_3$  formation [11,16,17]. On the other hand, Fig. 4b reveals that small equiaxed oxide grains (with diameter ranging from 1 to 2  $\mu\text{m}$ ) entirely cover the surface of the yttrium-containing alloy. This microstructure is typical of  $\alpha$ - $\text{Al}_2\text{O}_3$  [13,18]. These SEM observations are consistent with XRD patterns and confirm that fast oxide growth is related to the presence of transition aluminas and the low kinetic rate corresponds to  $\alpha$ -alumina.

### 3.4. SEM cross-sections and EDXS analyses

The SEM cross-sections of the oxidized specimens reveals that the oxide layer formed on the yttrium-free alloy (Fig. 5a) is thicker than the one developed on the yttrium-containing alloy (Fig. 5b). The thickness of the oxide layer formed on the yttrium-free alloy is about 2  $\mu\text{m}$ , which can be compared to the

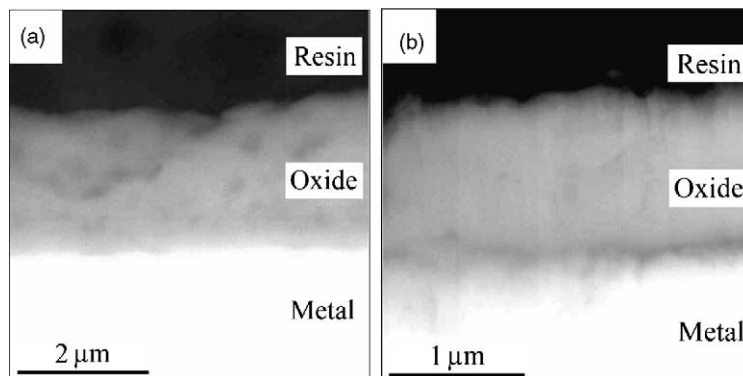


Fig. 5. SEM backscattered electron cross-section images of the oxide scales formed on Kanthal A1 (a), Kanthal AF (b), in air at 1173 K.

approximately 1  $\mu\text{m}$  thick oxide scale of the yttrium-containing alloy. These SEM observations can be related to the kinetic results, i.e. to the higher mass gains obtained after 120 h oxidation for the yttrium-free specimen than for the yttrium-containing alloy. The EDXS analyses of the oxide scales formed on Kanthal A1 and Kanthal AF (Figs. 6 and 7) show that mainly aluminium and oxygen are detected. In the

inner part, low intensity peaks of chromium and iron are detected, which is consistent with a contribution of the metal to the X-ray emission within the spotted region. Within the detection limit of EDXS (0.5 at.%), yttrium was not detected in the oxide scale formed on Kanthal AF. This corroborates the XRD results and suggests that yttrium compounds, if exist are present in very low amounts.

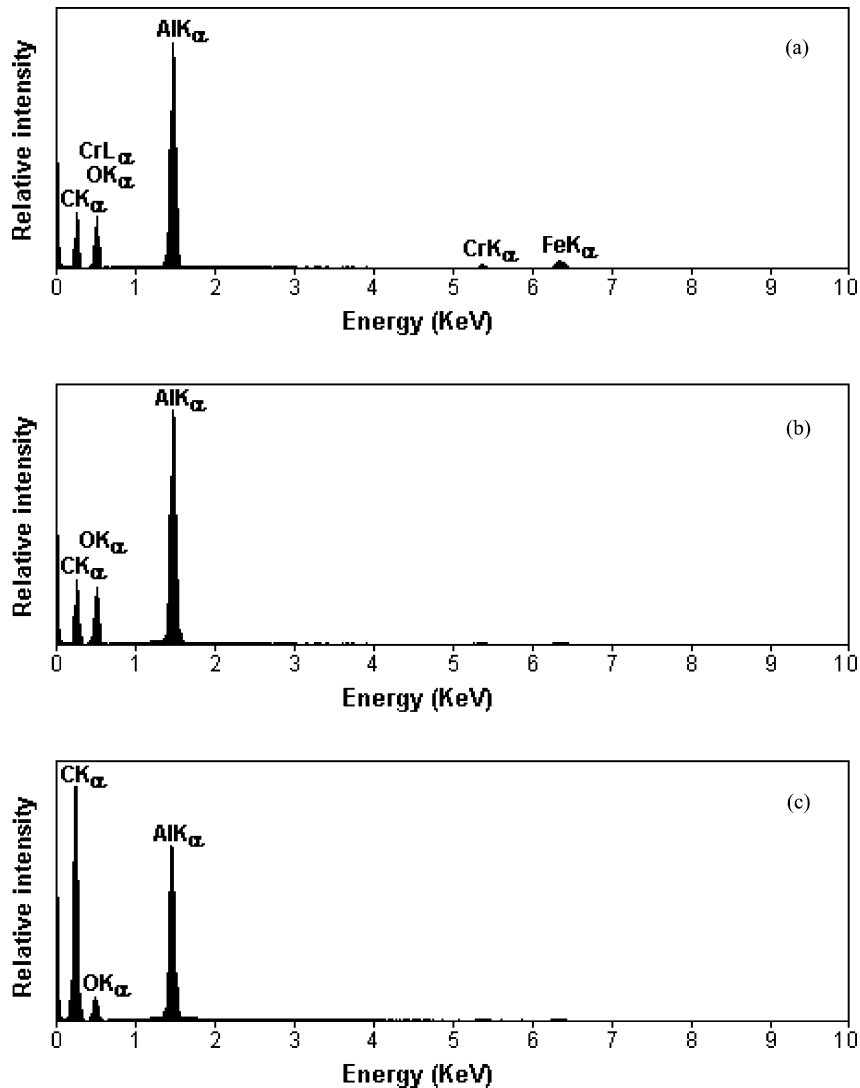


Fig. 6. EDXS spectra of the oxide scale formed on Kanthal A1: metal–oxide interface (a), intermediate part of the scale (b), and oxide–gas interface (c).

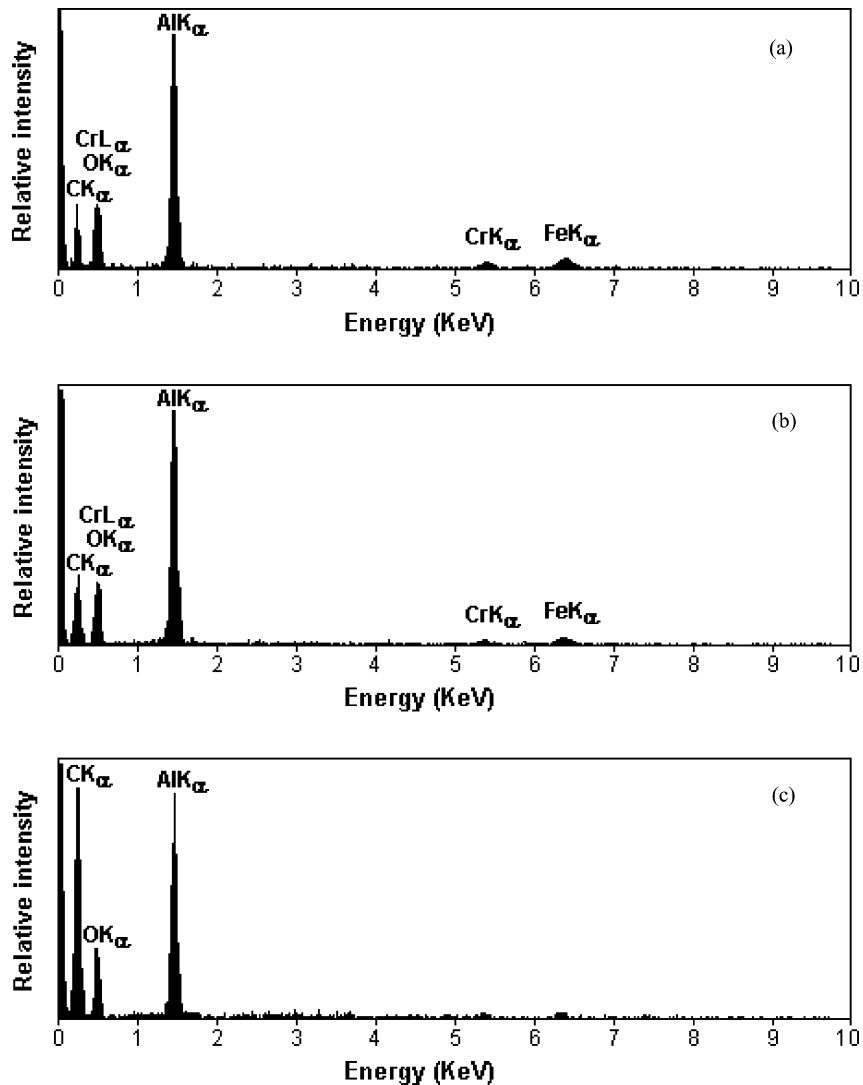


Fig. 7. EDXS spectra of the oxide scale formed on Kanthal AF: metal-oxide interface (a), intermediate part of the scale (b), and oxide-gas interface (c).

#### 4. Discussion

The steady-state stage of oxidation corresponds, for both alloys, to an oxidation process limited by diffusion through the growing oxide scale. The mass gain curves clearly show a marked influence of yttrium on the scale growth rate during this oxidation stage. The addition of the reactive element leads to a reduction of the parabolic rate constant by a factor of 10. Furthermore, the in situ XRD analysis revealed that transition

alumina is not detected in the oxide scale developed on the yttrium-doped alloy. These structural analyses correlated with kinetic studies suggest that the effect of the reactive element, by hampering the formation of transition aluminas or by leading to an acceleration of the phase transformation of transition aluminas into stable alumina, promotes the formation of a protective  $\alpha$ -Al $_2$ O $_3$  scale. This influence of the reactive element on the rate of transformation of metastable alumina into  $\alpha$ -alumina at temperatures below 1273 K is still a

matter of discussion. Some authors have reported that yttrium addition delays the phase transformation [11,19], whereas other investigations led to opposite conclusions, i.e. an acceleration of the rate of transformation [20,21]. A possible explanation of these various existing controversies is proposed by Jedlinski [22]. This author suggests that the influence of the reactive element can be accounted for in terms of several mechanisms, which lead to an acceleration or a retardation of the phase transformation. The relative contribution of each of these mechanisms depends on the amount and form of the reactive element [22]. Our results support the assumption that the involved mechanisms favour the formation of  $\alpha$ -Al<sub>2</sub>O<sub>3</sub>. This leads to a reduced mass gain since transition aluminas are less protective and faster growing than  $\alpha$ -alumina [12,23–25]. Other authors have also reported that yttrium as alloy element promotes the formation of stable  $\alpha$ -Al<sub>2</sub>O<sub>3</sub> [22,26]. They proposed that microstructural effects, involving additional sites for heterogeneous nucleation of the oxide as well as hampering the grain growth of unstable aluminas, may apply to the effect of small amounts of yttrium addition in the alloy. Earlier nucleation of the oxide layer results in accelerated evolution of the scale, and consequently, in earlier formation of the stable alumina [22]. Some authors have reported that the presence of titanium in alumina forming alloys could play a role in the phase transformation of transition alumina to  $\alpha$ -alumina [11–13]. Small additions of this element to the alloy would cause an acceleration of the phase transformation resulting in an early formation of stable  $\alpha$ -Al<sub>2</sub>O<sub>3</sub>. Since our study results are in agreement with the above assumption (Kanthal AF alloy contains the greatest amount of Ti and does not reveal the presence of transition alumina in the oxide scale), a possible effect of Ti on the phase transformation of alumina cannot be neglected.

It is well established that the growth mechanism of  $\alpha$ -alumina involves both inward oxygen diffusion and outward cation diffusion via short-circuit paths such as grain boundaries [27]. Some authors proposed that yttrium modifies the transport properties along the grain boundaries in  $\alpha$ -alumina scales [28,29]. These studies suggest that the lower parabolic rate constant observed with addition of yttrium is related to the reduction of the aluminium outward transport through the oxide scale. It has been also reported that reactive

elements have an important influence on the morphology of the scale. Several works have indicated that these elements can modify the grain size in the oxide scale. In many cases, it is mentioned that yttrium induces a decrease of the grain size of the alumina scale [18,30,31]. This indicates a change in the oxide growth process, which can affect the oxide growth rate and the mechanical properties (spallation resistance) of the oxide scale. Recently, the “dynamic segregation model” [32] established that the reactive element particles are not stagnant dopants in the grain boundaries but diffuse outward during scale growth, thus suggesting that the effect of the reactive element on the growth mechanism and on the scale microstructure is attenuated as the temperature increases. In the present study, the above theory of physical blocking of cation diffusion may rather play a minor role in the reactive element effect since the presence of yttrium in the oxide scale is probably very limited.

## 5. Conclusion

For both alloys, kinetic results clearly show that the oxide scale predominantly grows by a diffusional process (parabolic law) occurring after an initial transient stage of about 8 h. The lower oxidation rate registered during the parabolic stage of oxidation is the most significant effect resulting from the presence of alloying yttrium in Kanthal AF. The in situ XRD study revealed that this modification in oxidation kinetics can be related to a major structural change in the oxide scale composition, consisting in the absence of transition alumina in the oxide layer formed on the yttrium-containing alloy. This phenomenon, which has been established as part of the reactive element effect on the oxidation of alumina forming alloys, directly reflects the influence of yttrium in promoting the nucleation and growth of  $\alpha$ -alumina. As a consequence, the formation of a protective oxide scale occurs earlier on the yttrium-containing alloy than on the yttrium-free one.

## References

- [1] F.A. Golightly, F.H. Stott, G.C. Wood, *Oxid. Met.* 10 (1976) 163–187.

- [2] T.A. Ramanarayanan, R. Ayer, R. Petkovic-luton, D.P. Leta, *Oxid. Met.* 29 (1988) 445–472.
- [3] W.J. Quadackers, J. Jedlinski, K. Schmidt, M. Krasovec, G. Borchardt, H. Nickel, *Appl. Surf. Sci.* 47 (1991) 261–272.
- [4] H.J. Schmutzler, H. Viehhaus, H.-J. Grabke, *Surf. Interf. Anal.* 18 (1992) 581–584.
- [5] P.Y. Hou, J. Stringer, *Oxid. Met.* 38 (1992) 323–345.
- [6] D.R. Sigler, *Oxid. Met.* 40 (1993) 555–583.
- [7] J. Jedlinski, *Solid State Ionics* 101 (1997) 1033–1040.
- [8] C. Mennicke, E. Schumann, C. Ulrich, M. Ruhle, *Mater. Sci. Forum* 251–254 (1997) 389–396.
- [9] R. Prescott, D.F. Mitchell, J.W. Fraser, M.J. Graham, *J. Phys. IV* 3 (1993) 301–308.
- [10] E. Schumann, *Oxid. Met.* 43 (1995) 157–172.
- [11] B.A. Pint, J.R. Martin, L.W. Hobbs, *Solid State Ionics* 78 (1995) 99–107.
- [12] B.A. Pint, M. Treska, L.W. Hobbs, *Oxid. Met.* 47 (1997) 1–20.
- [13] K.M.N. Prasanna, A.S. Khanna, R. Chandra, W.J. Quadackers, *Oxid. Met.* 46 (1996) 465–480.
- [14] C. Badini, F. Laurella, *Surf. Coat. Technol.* 135 (2001) 291–298.
- [15] T. Biegun, M. Danielewski, Z. Skrzypek, *Oxid. Met.* 38 (1992) 207–215.
- [16] C. Mennicke, E. Schumann, M. Ruhle, R.J. Hussey, G.I. Sproule, M.J. Graham, *Oxid. Met.* 49 (1998) 455–466.
- [17] B.A. Pint, L.W. Hobbs, *J. Electrochem. Soc.* 141 (1994) 2443–2453.
- [18] M.W. Brumm, H.J. Grabke, *Corros. Sci.* 33 (1992) 1677–1690.
- [19] Y. Saito, B. Onay, T. Maruyama, *J. Phys. IV* 3 (1993) 217–230.
- [20] H.-J. Grabke, *Mater. Sci. Forum* 251–254 (1997) 149–161.
- [21] I. Rommerskirchen, V. Kolarik, *Mater. Corros.* 47 (1996) 625–630.
- [22] J. Jedlinski, *Oxid. Met.* 39 (1993) 55–60.
- [23] K.D.D. Lagerlof, B.J. Pletka, T.E. Mitchell, A.H. Heuer, *Radiat. Defects* 74 (1983) 87–107.
- [24] R. Prescott, M.J. Graham, *Oxid. Met.* 38 (1992) 73–87.
- [25] K. Messaoudi, A.M. Huntz, B. Lesage, *Mater. Sci. Eng. A* 247 (1998) 248–262.
- [26] J. Jedlinski, A. Glazkov, M. Konopka, G. Borchardt, E. Tscherkasova, M. Bronfin, M. Nocun, *Appl. Surf. Sci.* 103 (1996) 205–216.
- [27] F.H. Stott, *Mater. Sci. Forum* 251–254 (1997) 19–32.
- [28] B.A. Pint, J.R. Martin, L.W. Hobbs, *Oxid. Met.* 39 (1993) 167–195.
- [29] B.A. Pint, A.J. Garratt-Reed, L.W. Hobbs, *Mater. High Temp.* 13 (1995) 3–15.
- [30] M.K. Loudjani, C. Haut, *J. Eur. Ceram. Soc.* 16 (1996) 1099–1106.
- [31] M.K. Loudjani, C. Haut, S. Parisot, *Radiat. Effects Defects Solids* 134 (1995) 233–237.
- [32] B.A. Pint, *Oxid. Met.* 45 (1996) 1–37.